Simulation of linear isotropic Cosserat elasticity with conformally invariant curvature.

Jena Jeong[*] and Hamidreza Ramezani[†] and Ingo Münch [‡] and Patrizio Neff [§]

August 27, 2008

Abstract

We investigate the numerical response of the linear Cosserat model with conformal curvature. In our simulations we compare the standard Cosserat model with a novel conformal Cosserat model in torsion and highlight its intriguing features. In all cases, free boundary conditions for the microrotations $\overline{A}$ are applied. The size-effect response is markedly changed for the novel curvature expression. Our results suggest that the Cosserat couple modulus $\mu_c > 0$ remains a true material parameter independent of the sample size which is impossible for stronger, pointwise positive curvature expressions.

Key words: polar-materials, microstructure, conformal transformations
structured continua, solid mechanics, FEM.
**AMS 2000 subject classification: 74A35, 74A30, 74C05, 74C10
74C20, 74D10, 74E05, 74E10, 74E15, 74E20, 74G30, 74G65, 74N15**

Contents

[*]Corresponding author: Jena Jeong, Ecole Spéciale des Travaux Publics du Bâtiment et de l'Industrie (ESTP), 28 avenue du Président Wilson, 94234 Cachan Cedex, France, email: jena.jeong@univ-orleans.fr, Tel.: +33-2-38492465

[†]Hamidreza Adib-Ramezani, Ecole Polytechnique de l'Université d'Orleans, CNRS-CRMD, 8 rue Léonard de Vinci, 45072 Orleans, France, email: hamidreza.ramezani@univ-orleans.fr, Tel.: +33-2-38492465

[‡]Ingo Münch, Institut für Baustatik, Universität Karlsruhe (TH), Kaiserstr. 12 (Geb.10.50) , 76131 Karlsruhe, Germany, email: im@bs.uka.de, Tel.: +49-721 608 2289

[§]Patrizio Neff, AG6, Fachbereich Mathematik, Technische Universität Darmstadt, Schlossgartenstrasse 7, 64289 Darmstadt, Germany, email: neff@mathematik.tu-darmstadt.de, Tel.: +49-6151-16-3495

1   Introduction

The Cosserat continuum falls into the group of generalized continua which have the capacity to take into account size-effects in a natural manner. The Cosserat model is one of the most prominent extended continuum models. It has emerged from the work of the brothers Francois and Eugene Cosserat at the turn of the last century. Compared to classical linear elasticity the model features three additional, independent degrees of freedom, related to the rotation of each particle. In the simplest linear isotropic case, one coupling constant, here called Cosserat couple modulus $\mu_c \geq 0$ and three internal length scale parameters α, β, γ need to be determined in addition to the two classical Lamé-constants μ, λ. See[21, 18, 19, 9] for an in-depth discussion of mathematical and modelling aspects of the Cosserat model.[1]

In this work we will discuss the finite-element simulation of the linear Cosserat model with a hitherto not considered set of parameter values, called the conformal Cosserat case. The finite element analysis of Cosserat materials has already been studied in the literature. Early works on the finite element analysis based on the Cosserat theory are those done by Baluch [1] and Nakamura [17] in which a simple three-node triangle element with three degrees of freedom at each node is used for a two-dimensional problem. A higher-order triangle element again for a two-dimensional analysis based on Cosserat elasticity has been recently proposed by Providas [23], and Trovalusci et al.[28] treats the 2D-nonlinear case. The Cosserat theory has also been employed by Nadler and Rubin to formulate a three-dimensional finite element for dynamic analysis in nonlinear elasticity [16]. In addition, higher-order elements for elastic analysis of shells have been proposed by Jog [10]. Though several numerical studies have been conducted for Cosserat materials only few of them treat the full three-dimensional case. The two-dimensional Cosserat setting automatically removes two material parameters and the altogether required Cosserat material moduli reduce to only four (the two-dimensional problem is much simpler because of a fixed axis of rotations). An example calculation of the linear isotropic Cosserat model for two-dimensional finite elements has been performed by Li et al. [12]. There are also some studies in the literature for foams [2, 3, 24, 5, 4, 26, 7]. Huang et al. [8], Zastrau et al. [30, 31] have done very early attempts based on the Cosserat curvature parameter choice $\alpha = \beta = 0$, $\gamma > 0$ and $\beta = \gamma > 0$, $\alpha \geq 0$, respectively (see equation (1.2) for its meaning). Zastrau thus arrives at the symmetry of the couple stresses, a choice which has also been advocated as early as [27, 27, 25]. Recently the symmetry of the couple stress tensor has been motivated in [29] for the constraint couple stress model (the indeterminate couple stress model). In some cases, the algorithms are already extended to micropolar elasto-plastic problems, see, e.g. [13, 11, 20, 6]. First steps in the much more involved geometrically exact direction are taken in [15, 14].

While we have a geometrically exact 3D-code successfully running [15] we present here only the "linear" version for mainly two reasons: first, other groups do not necessarily have access to a 3D-geometrically exact code, making comparison impossible, and second, we investigate a novel situation, called the *conformal curvature case*, where already the linear response shows interesting features. Moreover, we solely concentrate on fully three-dimensional finite element models. Particularly, we focus on the torsion test with a cylindrical bar whose implementation helps us to take into account more pronounced size effects comparing to the simple tension, compression or three points bending test. Based on preliminary results of a yet unpublished paper [22] on the underlying theory of the conformal Cosserat model we infer that the weakest mathematically possible curvature energy assumption, still leading to a well-posed model, is a good choice. This not only reduces the needed Cosserat material moduli but also removes material moduli dependency problems which usually takes place for the stronger curvature energy assumption (pointwise positive "classical" case). By taking advantage of these theoretical findings we are motivated to put them into practice via our numerical experiments. As will be

---

[1]See also http://www.mathematik.tu-darmstadt.de/fbereiche/analysis/pde/staff/neff/patrizio/Cosserat.html

presented in the next sections, these experiments confirm the analytical aspects and provide a deep landscape on the Cosserat modeling and simulation issues.

Our paper is now organized as follows. First, we recall the variational setting of the Cosserat model, we present the weak form of the equations and give a classification for the Cosserat model introducing our novel conformal case. Then we establish universal analytical solutions for linear elasticity and conformal Cosserat elasticity which are further on used for the validation of our implementation. Next, we subject a planar beam network to a special, conformal mapping and compare its response to the Cosserat response. We present some details of our implementation and further validate it against the classical analytical torsion solution and other limit cases: linear elasticity and constant infinitesimal mean rotation. Having thus amply demonstrated the suitability of our methods we turn to the detailed investigation of size-effects in torsion for the different Cosserat curvature settings. The notation is found at the end.

Let us begin by establishing the linear Cosserat model along with some of our notation. This section does not contain new results.

1.1 The linear elastic Cosserat model in variational form

For the **displacement** $u : \Omega \subset \mathbb{R}^3 \mapsto \mathbb{R}^3$ and the **skew-symmetric infinitesimal microrotation** $\overline{A} : \Omega \subset \mathbb{R}^3 \mapsto \mathfrak{so}(3)$ we consider the **two-field** minimization problem

$$I(u, \overline{A}) = \int_\Omega W_{\mathrm{mp}}(\overline{\varepsilon}) + W_{\mathrm{curv}}(\nabla \operatorname{axl} \overline{A}) - \langle f, u \rangle \, \mathrm{dx} \mapsto \quad \min . \text{ w.r.t. } (u, \overline{A}), \qquad (1.1)$$

under the following constitutive requirements and boundary conditions

$$\overline{\varepsilon} = \nabla u - \overline{A}, \quad \textbf{first Cosserat stretch tensor}$$

$$u_{|_\Gamma} = u_{\mathrm{d}}, \quad \textbf{essential displacement boundary conditions}$$

$$W_{\mathrm{mp}}(\overline{\varepsilon}) = \mu \, \| \operatorname{sym} \overline{\varepsilon} \|^2 + \mu_c \, \| \operatorname{skew} \overline{\varepsilon} \|^2 + \frac{\lambda}{2} \operatorname{tr} [\operatorname{sym} \overline{\varepsilon}]^2 \qquad \textbf{strain energy}$$

$$= \mu \, \| \operatorname{sym} \nabla u \|^2 + \mu_c \, \| \operatorname{skew}(\nabla u - \overline{A}) \|^2 + \frac{\lambda}{2} \operatorname{tr} [\operatorname{sym} \nabla u]^2 \qquad (1.2)$$

$$= \mu \, \| \operatorname{dev} \operatorname{sym} \nabla u \|^2 + \mu_c \, \| \operatorname{skew}(\nabla u - \overline{A}) \|^2 + \frac{2\mu + 3\lambda}{6} \operatorname{tr} [\operatorname{sym} \nabla u]^2$$

$$= \mu \, \| \operatorname{sym} \nabla u \|^2 + \frac{\mu_c}{2} \, \| \operatorname{curl} u - 2 \operatorname{axl} \overline{A} \|_{\mathbb{R}^3}^2 + \frac{\lambda}{2} (\operatorname{Div} u)^2 \, ,$$

$$\phi := \operatorname{axl} \overline{A} \in \mathbb{R}^3, \quad \overline{\mathfrak{k}} = \nabla \phi, \quad \| \operatorname{curl} \phi \|_{\mathbb{R}^3}^2 = 4 \| \operatorname{axl} \operatorname{skew} \nabla \phi \|_{\mathbb{R}^3}^2 = 2 \| \operatorname{skew} \nabla \phi \|_{\mathbb{M}^{3 \times 3}}^2 \, ,$$

$$W_{\mathrm{curv}}(\nabla \phi) = \frac{\gamma + \beta}{2} \| \operatorname{sym} \nabla \phi \|^2 + \frac{\gamma - \beta}{2} \| \operatorname{skew} \nabla \phi \|^2 + \frac{\alpha}{2} \operatorname{tr} [\nabla \phi]^2 \qquad \textbf{curvature energy}$$

$$= \frac{\gamma + \beta}{2} \| \operatorname{dev} \operatorname{sym} \nabla \phi \|^2 + \frac{\gamma - \beta}{2} \| \operatorname{skew} \nabla \phi \|^2 + \frac{3\alpha + (\beta + \gamma)}{6} \operatorname{tr} [\nabla \phi]^2$$

$$= \frac{\gamma}{2} \| \nabla \phi \|^2 + \frac{\beta}{2} \langle \nabla \phi, \nabla \phi^T \rangle + \frac{\alpha}{2} \operatorname{tr} [\nabla \phi]^2$$

$$= \frac{\gamma + \beta}{2} \| \operatorname{sym} \nabla \phi \|^2 + \frac{\gamma - \beta}{4} \| \operatorname{curl} \phi \|_{\mathbb{R}^3}^2 + \frac{\alpha}{2} (\operatorname{Div} \phi)^2 \, .$$

Here, f are given volume forces while u_{d} are Dirichlet boundary conditions[2] for the displacement at $\Gamma \subset \partial \Omega$ where $\Omega \subset \mathbb{R}^3$ denotes a bounded Lipschitz domain. Surface tractions, volume couples and surface couples can be included in the standard way. The strain energy W_{mp} and the curvature energy W_{curv} are the most general isotropic quadratic forms in the **infinitesimal non-symmetric first Cosserat strain tensor** $\overline{\varepsilon} = \nabla u - \overline{A}$ and the **micropolar curvature tensor** $\overline{\mathfrak{k}} = \nabla \operatorname{axl} \overline{A} = \nabla \phi$ (curvature-twist tensor). The parameters μ, λ[MPa] are the classical Lamé moduli and α, β, γ are further micropolar moduli with dimension $[\mathrm{Pa} \cdot \mathrm{m}^2] = [\mathrm{N}]$ of a force.

The additional parameter $\mu_c \geq 0$[MPa] in the strain energy is the **Cosserat couple modulus**. For $\mu_c = 0$ the two fields of displacement u and microrotations $\overline{A} \in \mathfrak{so}(3)$ decouple and one is left formally with classical linear elasticity for the displacement u.

---

[2]Note that it is always possible to prescribe essential boundary values for the microrotations $\overline{A}$ but we abstain from such a prescription because the physics of it is misleading.

1.2 The weak form of the equilibrium balance equations

Let us recall the kinematic relation

$$\overline{\varepsilon} = \nabla u - \overline{A} \quad \text{with} \quad \overline{A} = -\varepsilon_{ijk}\phi_k, \tag{1.3}$$

along with the definition of the stress tensor σ and the couple stress tensor m

$$\sigma = \frac{\partial W_{\mathrm{mp}}(\overline{\varepsilon})}{\partial \overline{\varepsilon}}, \qquad m = \frac{\partial W_{\mathrm{curv}}(\nabla\phi)}{\partial \nabla\phi}. \tag{1.4}$$

The internal potential, Ψ_{int}, which is a functional of the non-symmetric infinitesimal Cosserat strain and curvature strain can be written as:

$$\Psi_{\mathrm{int}} = \int_\Omega W_{\mathrm{mp}}(\overline{\varepsilon}) + W_{\mathrm{curv}}(\nabla\phi)\,\mathrm{dV}. \tag{1.5}$$

Let W_{ext} define the external virtual work as below:

$$W_{\mathrm{ext}} = \int_\Omega \langle f, u\rangle + \langle M, \phi\rangle\,\mathrm{dV} + \int_{\partial\Omega} \langle f_s, u\rangle + \langle M_s, \phi\rangle\,\mathrm{dS}, \tag{1.6}$$

where f and M are the external body force and body moment. f_s and M_s are the stress vector and couple stress vector, respectively. Taking variations of the energy in (1.5) w.r.t. both displacement $u \in \mathbb{R}^3$ and infinitesimal microrotation $\overline{A} \in \mathfrak{so}(3)$ we arrive at the weak form of equilibrium system (the Euler-Lagrange equations of (1.1))

$$\delta\Psi_{\mathrm{int}} - \delta W_{\mathrm{ext}} = 0, \tag{1.7}$$

with

$$\delta\Psi_{\mathrm{int}} = \int_\Omega \langle D_{\overline{\varepsilon}}W_{\mathrm{mp}}(\overline{\varepsilon}), \delta\overline{\varepsilon}\rangle + \langle D_{\nabla\phi}W_{\mathrm{curv}}(\nabla\phi), \delta\nabla\phi\rangle\,\mathrm{dV}, \tag{1.8}$$

where $\delta\overline{\varepsilon} = \delta u - \delta\overline{A}$ is understood. With substitution of (1.8) and (1.6) into (1.7), the following equation is easily derived:

$$\int_\Omega \langle \sigma, \delta\overline{\varepsilon}\rangle + \langle m, \delta\nabla\phi\rangle\,\mathrm{dV} - \int_\Omega \langle f, \delta u\rangle + \langle M, \delta\phi\rangle\,\mathrm{dV} - \int_{\partial\Omega}\langle f_s, \delta u\rangle + \langle M_s, \delta\phi\rangle\,\mathrm{dS} = 0. \tag{1.9}$$

The virtual displacement δu is conjugate to the external force and the virtual rotation vector $\delta\phi$ to the external moment. This weak form is the basis for our numerical simulations.

1.3 The strong form of the linear elastic Cosserat balance equations

Going one step further we collect also the balance equations in strong form for our subsequent classification of the Cosserat model. Sorting (1.9) w.r.t. δu and $\delta\phi$ and using integration by parts we obtain

$$\begin{aligned}
\mathrm{Div}\,\sigma &= f, \qquad \textbf{balance of linear momentum} \\
-\mathrm{Div}\,m &= 4\,\mu_c \cdot \mathrm{axl\,skew}\,\overline{\varepsilon}, \quad \textbf{balance of angular momentum} \\
\sigma &= 2\mu \cdot \mathrm{sym}\,\overline{\varepsilon} + 2\mu_c \cdot \mathrm{skew}\,\overline{\varepsilon} + \lambda \cdot \mathrm{tr}\,[\overline{\varepsilon}] \cdot \mathbb{1} = (\mu + \mu_c) \cdot \overline{\varepsilon} + (\mu - \mu_c) \cdot \overline{\varepsilon}^T + \lambda \cdot \mathrm{tr}\,[\overline{\varepsilon}] \cdot \mathbb{1} \\
&= 2\mu \cdot \mathrm{dev\,sym}\,\overline{\varepsilon} + 2\mu_c \cdot \mathrm{skew}\,\overline{\varepsilon} + K \cdot \mathrm{tr}\,[\overline{\varepsilon}] \cdot \mathbb{1}, \\
m &= \gamma\,\nabla\phi + \beta\,\nabla\phi^T + \alpha\,\mathrm{tr}\,[\nabla\phi] \cdot \mathbb{1} \\
&= (\gamma + \beta)\,\mathrm{dev\,sym}\,\nabla\phi + (\gamma - \beta)\,\mathrm{skew}\,\nabla\phi + \frac{3\alpha + (\gamma + \beta)}{2}\,\mathrm{tr}\,[\nabla\phi]\,\mathbb{1}, \\
\phi &= \mathrm{axl}\,\overline{A}, \quad u_{|\Gamma} = u_{\mathrm{d}}.
\end{aligned} \tag{1.10}$$

We run this Cosserat model with three different sets of variables for the curvature energy which in each step relaxes the curvature energy.

1: **pointwise positive case:** $\frac{\mu L_c^2}{2}\|\nabla\phi\|^2$. This corresponds to $\alpha = 0, \quad \beta = 0, \quad \gamma = \mu L_c^2$.

2: **symmetric case:** $\frac{\mu L_c^2}{2}\|\,\mathrm{sym}\,\nabla\phi\|^2$. This corresponds to $\alpha = 0,\ \beta = \gamma$ and $\gamma = \frac{\mu L_c^2}{2}$.

3: **conformal case:** $\frac{\mu L_c^2}{2}\|\,\mathrm{dev\,sym}\,\nabla\phi\|^2 = \frac{\mu L_c^2}{2}(\|\,\mathrm{sym}\,\nabla\phi\|^2 - \frac{1}{3}\mathrm{tr}\,[\nabla\phi]^2)$. This corresponds to $\beta = \gamma$ and $\gamma = \frac{\mu L_c^2}{2}$ and $\alpha = -\frac{1}{3}\mu L_c^2$.

Note that all three cases are mathematically well-posed [9, 18]. The pointwise positive case1 is usually considered. Case2 leads to a symmetric couple-stress tensor which in turn has been considered by [30, 27, 27, 25] and case3 is the main object of our investigation.
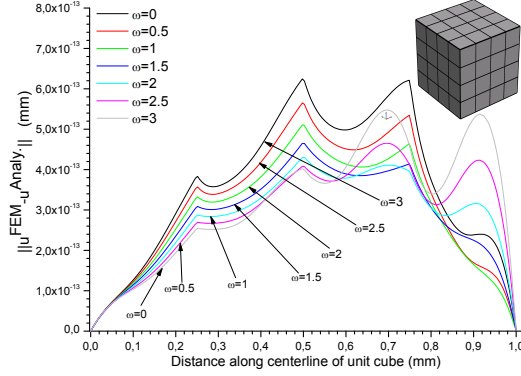
Figure 1: The difference of the linear Cauchy analytic solution and the approximated FEM solution for parameters $\widehat{W}_{12} = \widehat{W}_{13} = \widehat{W}_{23} = \omega \in \mathbb{R}$, $\widehat{A}_{12} = \widehat{A}_{13} = \widehat{A}_{23} = 1$ and $\widehat{b} = 0$ and DOFs= 2187 with quadratic elements.

2 Infinitesimal conformal transformations - universal solutions

Next we consider certain types of universal solutions, first for linear elasticity.

2.1 Linear elasticity and conformal invariance

The stress-strain relation in isotropic linear elasticity can always be written as

$$\sigma = 2\mu \cdot \operatorname{dev} \operatorname{sym} \nabla u + K \cdot \operatorname{tr}\left[\nabla u\right] \cdot \mathbb{1}\,, \tag{2.1}$$

where K is the bulk modulus. Inserting for u an **infinitesimal conformal map** u_C which is defined by

$$u_C(x) = \frac{1}{2}\left(2\langle\operatorname{axl}(\widehat{W}), x\rangle\, x - \operatorname{axl}(\widehat{W})\,\|x\|^2\right) + [\widehat{p}\,\mathbb{1} + \widehat{A}].x + \widehat{b}\,,$$
$$\nabla u_C(x) = \operatorname{anti}(\widehat{W}.x) + \langle\operatorname{axl}(\widehat{W}), x\rangle\, \mathbb{1} + (\widehat{p}\,\mathbb{1} + \widehat{A})\,, \tag{2.2}$$

where $\widehat{W}, \widehat{A} \in \mathfrak{so}(3)$, $\widehat{b} \in \mathbb{R}^3$ and $\widehat{p} \in \mathbb{R}$ are arbitrary constants, we have for the Cauchy stress

$$\sigma(\nabla u_C) = 2\mu \cdot 0 + K \operatorname{tr}\left[\nabla u_C\right]\mathbb{1} = K \operatorname{tr}\left[\widehat{p} + \langle\operatorname{axl}(\widehat{W}), x\rangle\,\mathbb{1}\right]\mathbb{1} = 3\,K\left(\widehat{p} + \langle\operatorname{axl}(\widehat{W}), x\rangle\right)\mathbb{1}.$$

Thus $\operatorname{Div}\sigma(\nabla u_C) = 3\,K\,\operatorname{axl}(\widehat{W})$, for $\widehat{p}$ is constant and $\operatorname{Div}[\langle\widehat{k}, x\rangle\mathbb{1}] = \widehat{k}$. Since the linear boundary value problem

$$\operatorname{Div}\sigma(\nabla u) = 3\,K\,\operatorname{axl}(\widehat{W})\,, \quad u_{|_\Gamma}(x) = u_C(x)\,, \tag{2.3}$$

for a given constant $\widehat{W} \in \mathfrak{so}(3)$ admits a unique solution, this solution is already given by $u(x) = u_C(x)$. We have therefore obtained an inhomogeneous, three-dimensional analytical solution for the boundary value problem of linear elasticity with constant body forces $\widehat{f} = 3\,K\,\operatorname{axl}(\widehat{W})$. This solution can be profitably used to check any numerical algorithm for linear Cauchy elasticity. In our case we consider one unit cube to check the numerical exactness obtained by us. The analytical conformal solution u_C of the boundary value problem (2.3) is compared against the simulation and the error $(\|u^{FEM} - u^{Analy.}\|_{\mathbb{R}^3})$ is plotted in Figure 1. We have reached complete agreement.

Remark 2.1 (Application to infinitesimal elasto-plasticity)
The proposed analytical solution is on the one hand quite inhomogeneous, on the other hand it holds that $\operatorname{dev}\sigma \equiv 0$. Therefore, classical numerical approaches for plasticity with von Mises flow laws should not give any plastic response since the yield stress is never reached. This can serve as a nontrivial numerical test for any algorithm for plasticity, especially, if the shear modulus $\mu(x)$ is assumed to have large jumps [20].

5
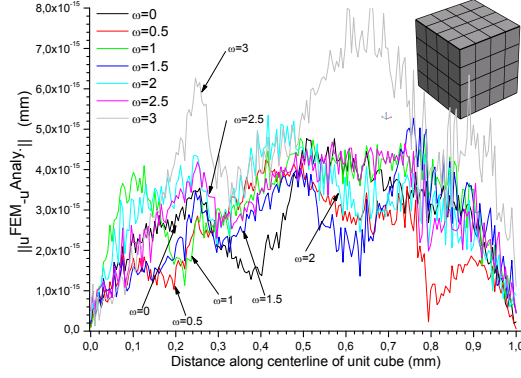
Figure 2: Error of FEM-solution against the analytical solution for the conformal Cosserat case with $\widehat{W}_{12} = \widehat{W}_{13} = \widehat{W}_{23} = \omega \in \mathbb{R}$, $\widehat{p} = 1$, $\widehat{A}_{12} = \widehat{A}_{13} = \widehat{A}_{23} = 1$ and $\widehat{b} = 0$, DOFs= 4374, quadratic elements.

2.2 Linear Cosserat elasticity and conformal invariance

An extraordinary feature of this type of conformal solution in linear elasticity is that it is a universal solution for the Cosserat model and the indeterminate couple stress model as well, if the conformal curvature expression (case3) is used. The solution is invariant of the Cosserat coupling constant μ_c and the internal length scale L_c.[3] To understand this claim let us consider the boundary value problem of linear Cosserat elasticity in strong form with conformal curvature (case3):

$$\operatorname{Div} \sigma(\nabla u, \overline{A}) = \widehat{f}, \quad -\operatorname{Div} m = 4\mu_c \cdot \operatorname{axl}(\operatorname{skew} \nabla u - \overline{A}), \tag{2.4}$$
$$\sigma = 2\mu \cdot \operatorname{dev} \operatorname{sym} \nabla u + 2\mu_c \cdot \operatorname{skew}(\nabla u - \overline{A}) + K \cdot \operatorname{tr}[\nabla u] \cdot \mathbb{1},$$
$$m = \mu L_c^2 \cdot \operatorname{dev} \operatorname{sym} \nabla \operatorname{axl}(\overline{A}), \quad u_{|\partial\Omega} = u_C,$$

where $\widehat{f}$ and u_C are taken from (2.1). We proceed to show that the solution of this boundary value problem is uniquely given by

$$u(x) = u_C(x), \qquad \overline{A}(x) = \operatorname{anti}(\frac{1}{2} \operatorname{curl} u(x)), \tag{2.5}$$

independent of $\mu(x)$, $\mu_c(x)$ and $L_c(x)$. To see this, consider

$$\operatorname{skew}(\nabla u - \overline{A}) = \operatorname{anti}(\operatorname{axl}(\operatorname{skew} \nabla u - \overline{A})) = \operatorname{anti}(\frac{1}{2} \operatorname{curl} u - \operatorname{axl}(\overline{A})). \tag{2.6}$$

Choosing $\overline{A}(x) = \operatorname{anti}(\frac{1}{2} \operatorname{curl} u(x))$ simplifies the equations to

$$\operatorname{Div}\sigma(\nabla u, \overline{A}) = \widehat{f}, \quad -\operatorname{Div} m = 0, \tag{2.7}$$
$$\sigma = 2\mu \cdot \operatorname{dev} \operatorname{sym} \nabla u + K \cdot \operatorname{tr}[\nabla u] \cdot \mathbb{1}, \qquad m = \mu L_c^2 \operatorname{dev} \operatorname{sym} \nabla[\frac{1}{2} \operatorname{curl} u(x)].$$

Since $u = u_C$ and u_C is conformal, it follows [22] that the couple stress or so called moment stress tensor vanishes, $m \equiv 0$. The remaining equation for the force stresses σ is satisfied because of (2.3). Since we have used $\overline{A}(x) = \operatorname{anti}(\frac{1}{2} \operatorname{curl} u(x))$, the obtained solution is also a solution for the indeterminate couple stress problem (which corresponds formally to setting $\mu_c = \infty$). ∎

Based on the above-mentioned constitutive equations for the stress, couple stress and the applied conformal boundary condition on the unit cube, the numerical exactness of our algorithm for Cosserat elasticity (see below) has also been checked: the generic error ($\|u^{FEM} - u^{Analy.}\|_{\mathbb{R}^3}$) comparing against the analytical Conformal solution u_C is shown in Figure 2. The maximum error is less than 10^{-14} for the displacement vector and 5×10^{-13} for the microrotation vector (without figure), respectively.

---

[3]Here, even a strong variation in shear modulus $\mu(x)$ would be allowed (as well as a strong variation in the couple modulus $\mu_c(x)$ and internal length scale $L_c(x)$. Only the bulk modulus K must be constant.
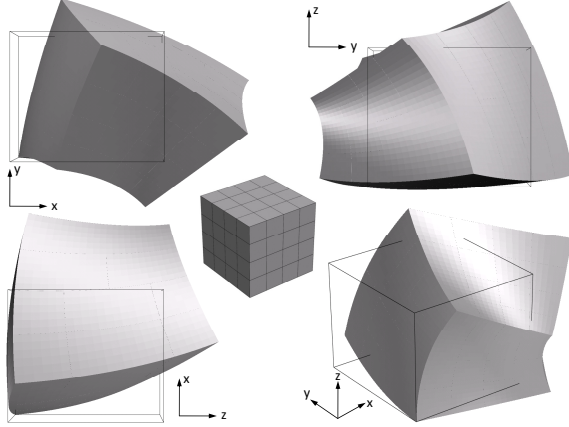
Figure 3: Deformed and undeformed shape of the unit cube under infinitesimal conformal transformation u_C as boundary condition using the linear elastic Cosserat method and case3 assumption with $\widehat{W}_{12} = \widehat{W}_{13} = \widehat{W}_{23} = 3$, $\widehat{p} = -4$, $\widehat{A}_{12} = \widehat{A}_{13} = \widehat{A}_{23} = 4$ and $\widehat{b} = 0$, DOFs= 4300, quadratic elements.

In Figure 3, the infinitesimal conformal map u_C is taken as boundary condition and the deformed cube, computed for the conformal Cosserat model is shown, depicting the inhomogeneity of the conformal solutions. Note that it is not necessary to apply the displacement-boundary condition u_C everywhere at $\partial\Omega$ in order to obtain u_C as solution of the boundary value problem.

3   A beam network versus the conformal Cosserat model

To gain further understanding of the conformal Cosserat model, case3, we subject a regular and rectangular network of beams to an infinitesimal conformal displacement. The infinitesimal conformal displacement is taken as in $(2.2)_1$ as

$$u_C(x) = \frac{1}{2}\left(2\langle\mathrm{axl}(\widehat{W}), x\rangle\, x - \mathrm{axl}(\widehat{W})\, \|x\|^2\right) + [\widehat{p}\,\mathbb{1} + \widehat{A}].x + \widehat{b}\,, \qquad (3.1)$$

where $\widehat{W}$, $\widehat{A} \in \mathfrak{so}(3)$, $\widehat{b} \in \mathbb{R}^3$, $\widehat{p} \in \mathbb{R}$ are given constant parameters. In our comparison we use $\widehat{b} = 0$, $\widehat{A} = 0$ and some generic values for $\widehat{p}$ and $\widehat{W}$. The area of the squared structure is 1 and the beams are characterized by a quadratic cross section with dimension 0.05. Thus, the area of the cross section amount to 0.0025 and the moment of inertia to $5.208 \cdot 10^{-7}$ against bending. The Young's modulus is set to $E = 1$. We use the Bernoulli beam theory of second order. Thus, displacements and rotations are limited to a reasonable amount.

First, only nodes on the boundary are conformally displaced, all other organize itself by minimizing strain and curvature energy of the beams. In Figure 4, one can see the initial rectangular beam structure, the boundary conditions and the displacement vectors bringing all nodes of the boundary into the conformally corresponding points. The nodes within the structure meet the condition, that for all beams balance of momentum and balance of angular momentum is fulfilled. The right picture in Figure 4 indicates, that nearly everywhere in all beams curvature appears. The maximum value of this curvature is about 6.24.

Now, all nodes of the structure are conformally displaced. Thus, only the curvature energy of the beams can be minimized. In Figure 5, one can see the initial rectangular beam structure, the boundary conditions and the displacement vectors bringing all nodes into their conformally corresponding points. The beams satisfy balance of angular momentum. The right picture in Figure 5 indicates, that also nearly everywhere in all beams curvature appears. The maximum value of this curvature is about 7.02.

While the infinitesimal conformal mapping does not give rise to a curvature contribution in the Cosserat model with conformal curvature (case3), we clearly see that the beams-network response is always with curvature. This allows us to already conclude that *the conformal Cosserat model cannot be identified with a homogenized beam model.* We rather expect a homogenized
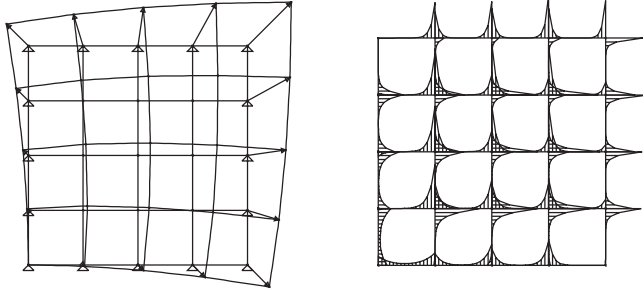
Figure 4: Left: Initial structure with boundary conditions, displacement vectors and deformed mesh. Right: Trend of curves (plotted on undeformed mesh) indicates the curvature of beams.
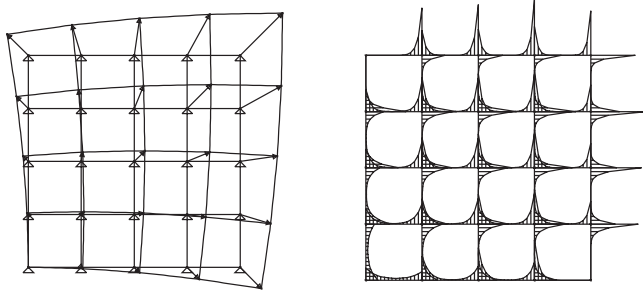
Figure 5: Left: Initial structure with boundary conditions, displacement vectors and deformed mesh. Right: Trend of curves (plotted on undeformed mesh) indicates the curvature of beams.

beam model to give rise to a uniform positive definite curvature expression as embodied in case1 of our classification.

4 Finite element analysis

4.1 Preliminaries and assumptions

The finite element method has been chosen as a relevant numerical method for the linear elastic Cosserat model. We use **isometric Lagrange shape functions** in our study. Moreover, we use quadratic Lagrange shape function for the displacements u and linear Lagrange shape functions for the entries of the microrotation $\overline{A} \in \mathfrak{so}(3)$. According to the discussed balance equations, there are six available state variables (three for the displacement vector u and three for micro rotation vector $\mathrm{axl}(\overline{A})$) whose computations need to be done via the coupled linear partial differential system of equations using the momentum and angular momentum balance equations based upon the weak form. We consider a cylindrical bar (diameter$= 2mm$, height$= 10mm$) submitted to the torsion angle θ at the end and choose the e_3-axis to coincide with the axis in Figure 6, where the assumed classical, size-independent parameters E, ν can be found.

Remark 4.1 (Ansatz functions)
In all test cases we use quadratic ansatz functions for displacements u and linear ansatz function for microrotations $\overline{A}$. We expect a significant improvement of the accuracy of the numerical solution provided we use quadratic ansatz functions for the displacement and linear ansatz functions for the microrotations $\overline{A}$ since in the coupling term we have $\mu_c \, \| \, \mathrm{skew} \, \nabla u - \overline{A} \|^2$ whose summands thus have both the same order of approximation.

All our computations have been prepared by means of a user-written code within the general purpose FEM software COMSOL (formerly FEMLAB). We have used a parallelized direct solver making it possible to reduce the computation runtime and to enable us to utilize the full capacity of the available hardware; here an AMD-System with 8 GB memory and dual core 3 Ghz processor has been used. A computation with 550.000 DOFs would last 4 days. As will be seen later, our numerical results clearly show the qualitatively new behavior of the linear

8

Young's modulus (MPa)	Poisson's ratio (-)
1E6	0.30
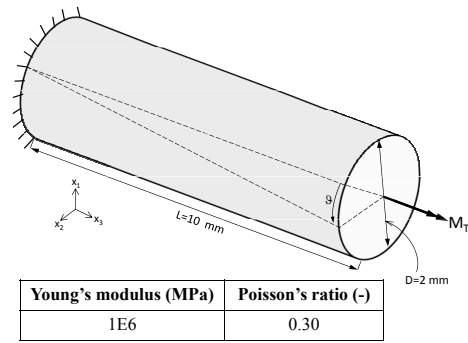
Figure 6: The geometry and data of the torsion problem for our implementation.

Number of elements	Type of elements	DOFs
6912	Hexahedral	198 618
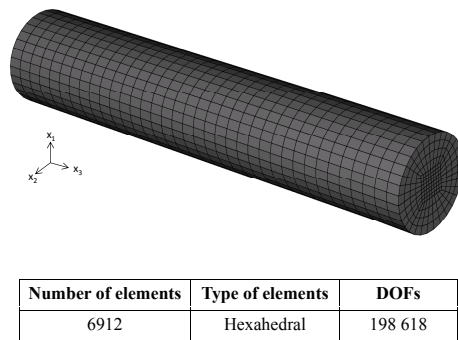
Figure 7: Mesh density illustration and mesh statistics for considered circular bar (Fig. 6).

Cosserat model for our relaxed conformal curvature energy expression, case3. In contrast to the pointwise positive definite curvature energy (case1) and the symmetric case2 our relaxed energy provides a completely different spectrum of size-dependent behavior. This is what we expected on theoretical grounds but which is also neatly covered by our numerical experiments.

In order to further validate our simulations, we run first the linear elastic Cauchy response, which is included in the Cosserat model by setting $\mu_c > 0$ and $L_c = 0$. Then we slightly increase $L_c > 0$ to still observe comparable qualitative response. The results for the torque computation are also compared to the results of Münch [15]. Since [15] is set up entirely in terms of geometrically exact expressions we use, for comparison purposes a nonlinear evaluation formula for the stresses and an adapted application of boundary conditions in order to get as close as possible from our linear model to the geometrically exact development. This procedure is detailed next.

4.2 Geometrically exact application of torsion angle

We propose an evaluation of the stresses which will be as far as possible be consistent with geometrically exact strain measures, only the first Piola-Kirchhoff stresses S_1 will derive from a quadratic potential $W(F)$, thus ultimately destroying geometrical exactness.

Let us summarize the necessary relations. The first Piola-Kirchhoff stresses in nonlinear elasticity are given by

$$S_1(F) = D_F W(F) = \det[F]\, \sigma^{\text{exact}}\, F^{-T}\,, \tag{4.1}$$

where $F = \nabla\varphi = \mathbb{1} + \nabla u$ is the deformation gradient and ∇u the displacement gradient and the exact Cauchy stress σ^{exact} follows as usual from (4.1)

$$\sigma^{\text{exact}}(F) = \frac{1}{\det[F]}\, S_1(F)\, F^T\,. \tag{4.2}$$

The same definitions apply, with appropriate changes, also to the Cosserat model. Thus we have two possibilities to calculate the stresses either according to the linear Cosserat model or by linear Cauchy elasticity.

Recalling the energy contributions (W_{mp} for Cosserat linear elasticity and W_{lin} for classical linear elasticity) giving rise to the classical stresses, we have

$$W_{\text{mp}}(\overline{\varepsilon}) = \mu\|\operatorname{sym}\overline{\varepsilon}\|^2 + \mu_c\|\operatorname{skew}\overline{\varepsilon}\|^2 + \frac{\lambda}{2}\operatorname{tr}[\overline{\varepsilon}]^2\,, \qquad W_{\text{lin}}(\varepsilon) = \mu\,\|\varepsilon\|^2 + \frac{\lambda}{2}\operatorname{tr}[\varepsilon]^2\,, \tag{4.3}$$

where the applied kinematic relation for each case is:

$$\overline{\varepsilon} = \nabla u - \overline{A} = F - \mathbb{1} - \overline{A}\,, \qquad \varepsilon = \operatorname{sym}\nabla u = \operatorname{sym}(F - \mathbb{1})\,. \tag{4.4}$$

This leads to the respective first Piola-Kirchhoff stresses S_1^{mp} for Cosserat linear elasticity and S_1^{lin} for classical linear elasticity, i.e.,

$$\begin{aligned} S_1^{\text{mp}}(F,\overline{A}) &= D_F W_{\text{mp}}(F,\overline{A}) \\ &= 2\mu\,(\operatorname{sym} F - \mathbb{1} - \overline{A}) + 2\mu_c\operatorname{skew}(F - \mathbb{1} - \overline{A}) + \lambda\operatorname{tr}\left[\operatorname{sym} F - \mathbb{1} - \overline{A}\right]\mathbb{1}\,, \\ S_1^{\text{lin}}(F) &= D_F W_{\text{lin}}(F) = 2\mu\,(\operatorname{sym} F - \mathbb{1}) + \lambda\operatorname{tr}\left[\operatorname{sym} F - \mathbb{1}\right]\mathbb{1}\,. \end{aligned} \tag{4.5}$$

Inserting $S_1^{\text{lin}}(F)$ into the Cauchy stress formula (4.2) we obtain the our Cauchy stresses in the actual configuration from

$$\begin{aligned} &\sigma^{\text{exact}}(F) \\ &= \frac{1}{\det[F]}\, S_1^{\text{lin}}(F)\, F^T = \frac{1}{\det[F]}\,\left(2\mu\,(\operatorname{sym} F - \mathbb{1}) + \lambda\operatorname{tr}\left[\operatorname{sym} F - \mathbb{1}\right]\mathbb{1}\right) F^T \\ &= \frac{1}{\det[\mathbb{1} + \nabla u]}\,\left(2\mu\,(\varepsilon + \lambda\operatorname{tr}[\varepsilon]\,\mathbb{1}\right)(\mathbb{1} + \nabla u)^T = \frac{1}{\det[\mathbb{1} + \nabla u]}\,\sigma^{\text{lin}}(\varepsilon)\,(\mathbb{1} + \nabla u)^T\,, \end{aligned} \tag{4.6}$$

and similarly for S_1^{mp}. This formula for σ^{exact} will be used in the evaluation of the torque in (4.12). The torsion problem which we are going to consider gives rise to an inhomogeneous deformation field which makes it a fundamental test for each Cosserat model, small strain or finite strain. This holds since the Cosserat curvature expression is invariably activated. Despite
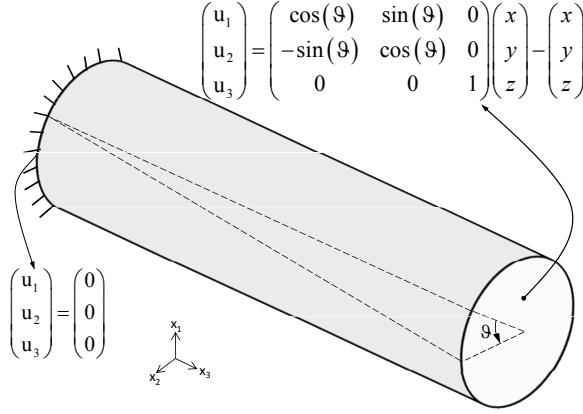
Figure 8: Boundary conditions for the circular bar, clamped at the bottom and rotated at the top of cylinder by an exact rotation with angle ϑ.

the fact that we deal with a linear Cosserat model we **apply an exact rotation** at the upper face (at height L) of the sample with angle ϑ given by

$$
\begin{pmatrix} \cos\vartheta & \sin\vartheta & 0 \\ -\sin\vartheta & \cos\vartheta & 0 \\ 0 & 0 & 1 \end{pmatrix} = \mathbb{1} + \begin{pmatrix} 0 & \vartheta & 0 \\ -\vartheta & 0 & 0 \\ 0 & 0 & 0 \end{pmatrix} + \dots . \tag{4.7}
$$

4.3 Analytical torsion solution for circular cross-section without warping and linear boundary condition

If in the torsion problem the sample has circular cross-section with diameter $D = 2r$ and height L, then an analytical solution for the linear Cauchy-elastic problem is available which connects the rotation at the upper face with the applied angle. In this special case, the cross-sections remain plane (no warping) and each cross section is rotated along the torsion axis. Since we deal with a linear problem, the rotation angle in height z along the torsion axis is proportional to z. In terms of the deformation we have

$$
\varphi_L(x,y,L) = \begin{pmatrix} x \\ y \\ L \end{pmatrix} + A_L . \begin{pmatrix} x \\ y \\ L \end{pmatrix}, \quad A_L = \begin{pmatrix} 0 & \vartheta & 0 \\ -\vartheta & 0 & 0 \\ 0 & 0 & 0 \end{pmatrix}, \text{ boundary condition at upper face}
$$

$$
\varphi(x,y,z) = \begin{pmatrix} x \\ y \\ z \end{pmatrix} + \begin{pmatrix} \frac{\vartheta}{L} y z \\ -\frac{\vartheta}{L} x z \\ 0 \end{pmatrix}, \quad \text{deformation solution} . \tag{4.8}
$$

It is simple to see that the Dirichlet boundary conditions $\varphi(x,y,0) = (x,y,0)$ (fixed at the bottom) and $\varphi(x,y,L) = \varphi_L(x,y,L)$ (infinitesimally rotated at upper face) are satisfied. Moreover, φ satisfies the linear elasticity equations. Therefore we get for the displacement

$$
u(x,y,z) = \begin{pmatrix} \frac{\vartheta}{L} y z \\ -\frac{\vartheta}{L} x z \\ 0 \end{pmatrix}, \ \nabla u = \begin{pmatrix} 0 & \frac{\vartheta}{L} z & \frac{\vartheta}{L} y \\ -\frac{\vartheta}{L} z & 0 & -\frac{\vartheta}{L} x \\ 0 & 0 & 0 \end{pmatrix}, \ \text{skew}\,\nabla u = \begin{pmatrix} 0 & \frac{\vartheta}{L} z & \frac{\vartheta}{2L} y \\ -\frac{\vartheta}{L} z & 0 & -\frac{\vartheta}{2L} x \\ -\frac{\vartheta}{2L} y & \frac{\vartheta}{2L} x & 0 \end{pmatrix},
$$

$$
\text{sym}\,\nabla u = \begin{pmatrix} 0 & 0 & \frac{\vartheta}{2L} y \\ 0 & 0 & -\frac{\vartheta}{2L} x \\ \frac{\vartheta}{2L} y & -\frac{\vartheta}{2L} x & 0 \end{pmatrix} . \tag{4.9}
$$

11
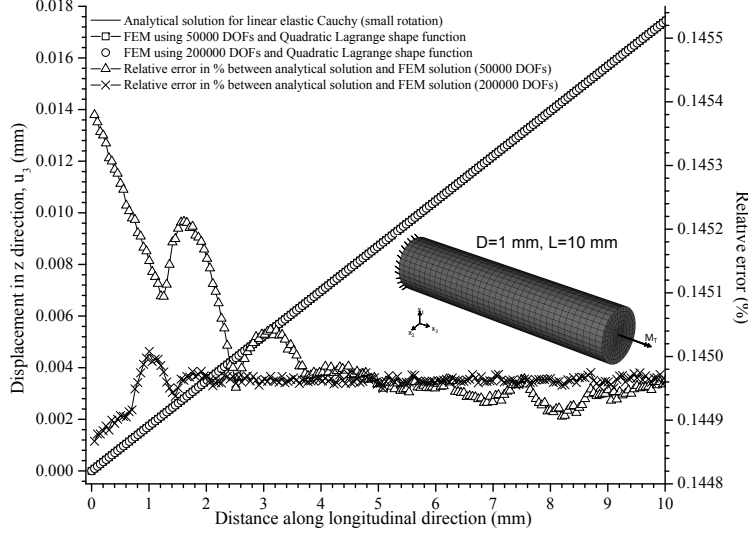
Figure 9: Comparison between the analytical solution and FEM solution using 50000 DOFs and 200000 DOFs for the displacement in x direction, u_1 versus distance along longitudinal direction of chosen cylindrical bar including relative error in percentage ($\vartheta = 2° = \frac{\pi}{90}\,rad.$)

For very small angles θ we may compare this (completely linear)[4] against our FEM solution which has been calculated on the basis of (4.7).

The comparison among the above-mentioned analytical solution and those found for the linear elastic Cauchy model are illustrated in Figure 9, Figure 10 including relative error for very small angle ($2° = \frac{\pi}{90}\,rad.$). The finite element analyses are performed for two different DOFs, i.e., 50000 DOFs and 200000 DOFs. Using **Dirichlet boundary conditions** at the upper face of the cylindrical bar allows us to apply the geometrically exact angles even for large rotation angles. The relative error obtained via FEM are very small and show that the numerical and analytical results for small rotation angles match perfectly. As previously mentioned, the numerical simulations for displacement component in x-direction well agrees with the analytical solution. Evidently, these comparisons are valid only for fairly small angles ($\vartheta < 6° = \frac{\pi}{30}$ rad.). The comparison between these situations confirms this margin for the torsion tests.

For given applied rotation angle ϑ at the upper face we have

$$M_T = \frac{G\,I_T}{L}\,\vartheta\,,\quad I_T = \frac{\pi}{2}\,r^4 = \frac{\pi\,D^4}{32}\,,\quad G = \mu = \frac{E}{2\,(1+\nu)}\,. \tag{4.10}$$

Here, M_T is the applied torque, I_T is the torsion coefficient (here the polar moment of inertia) and $G = \mu\,[\frac{N}{mm^2}]$ is the shear modulus. The torque about the e_3-axis at the upper surface $\partial\Omega^+$ is given by the following classical formula

$$M_T^{\mathrm{lin}} = \int_{\partial\Omega^+} (x\,\sigma_{32}^{\mathrm{lin}} - y\,\sigma_{31}^{\mathrm{lin}})\,\mathrm{dx}\,\mathrm{dy} = \mu\,\frac{\vartheta}{L}\int_{\partial\Omega^+} (x^2 + y^2)\,\mathrm{dx}\,\mathrm{dy} = \mu\,\frac{\vartheta}{L}\,I_T\,, \tag{4.11}$$

where we have used σ^{lin} according to (4.9). In addition, the applied torque based on the obtained exact Cauchy stresses (4.6) will be defined as follows

$$M_T^{\mathrm{exact}} = \int_{\partial\Omega^+} (x\,\sigma_{32}^{\mathrm{exact}} - y\,\sigma_{31}^{\mathrm{exact}})\,\mathrm{dx}\,\mathrm{dy}\,. \tag{4.12}$$

In the present paper, we obtain the torque value by integration on the upper surface of the cylindrical bar using (4.12) for the applied angles ($0 \le \vartheta \le \frac{20\pi}{180}\,rad.$). The torque-torsion angle curve is plotted in Figure 11. As illustrated in Figure 11, the analytic solution differs from the calculated solution for larger torsion angles.

---

[4]In the linear analytic solution the boundary condition is applied linearly in θ. All our simulations are based, however, on prescribing exact rotations at the upper face. There, both $\cos\theta$ and $\sin\theta$ are used. While a Taylor series approximation for trigonometric functions of $\sin\theta = \theta - \frac{\theta^3}{3!} + \frac{\theta^5}{5!} - \ldots$ is acceptable for $|\theta| \le \frac{\pi}{30}rad$ the approximation $\cos\theta = 1 - \frac{\theta^2}{2!} + \frac{\theta^4}{4!} \ldots$ is only useful for $|\theta| \le \frac{\pi}{30}rad$ with a maximal relative error 0.5478 percent for $\sin\theta$ and 0.183 for $\cos\theta$.
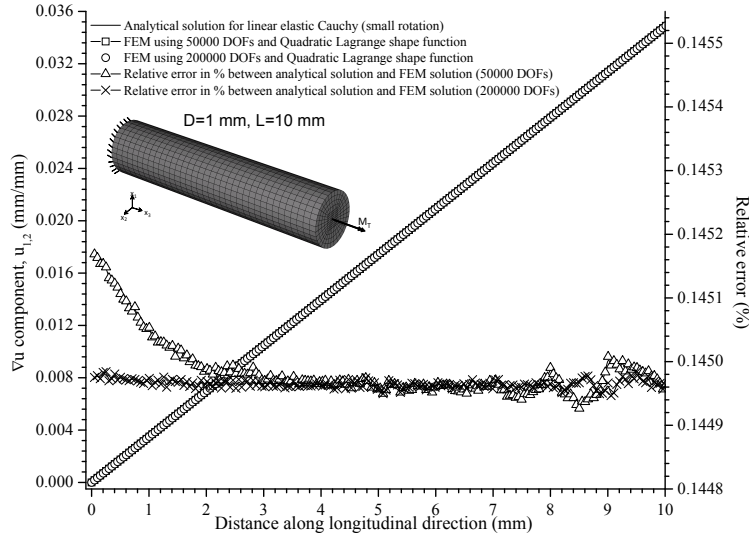
Figure 10: Comparison between the analytical solution and FEM solution using 50000 DOFs and 200000 DOFs for a displacement gradient component $u_{1,2}$ versus distance along longitudinal direction of the cylindrical bar including relative error in percentage for $\vartheta = 2° = \frac{\pi}{90}\,rad$.
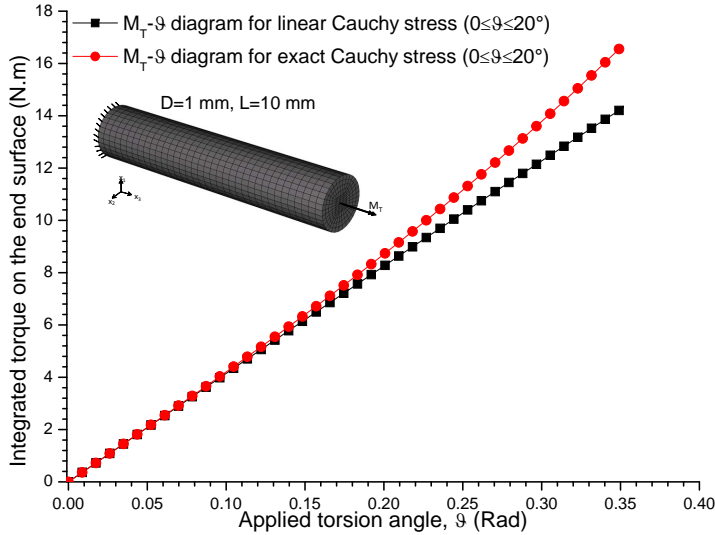
Figure 11: Torque-torsion angle diagram for the geometrically exact Cauchy stress and linear Cauchy stress ($0 \leq \vartheta \leq 20°$). Calculation based on Cosserat kinematics with $\mu_c > 0$ and $L_c = 0$.
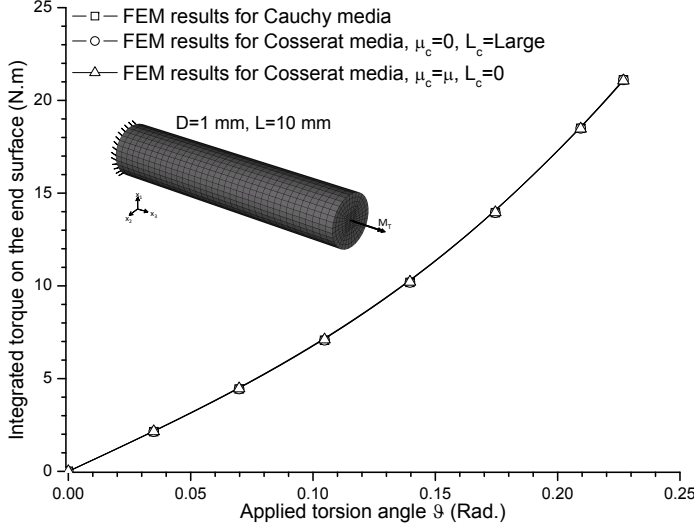
Figure 12: Comparison among the Cauchy media, Cosserat case limit 1 ($\mu_c = 0$, L_c=Large) and Cosserat case limit 2 ($\mu_c = \mu$, $L_c = 0$) for $0 \leq \vartheta \leq 13°$. Calculation based on Cosserat kinematics.

5 Consistency of the implementation

In order to increase further confidence in our numerical algorithm we check next various other limiting cases, where the analytical solution can be read off at once.

5.1 Limit case: Cauchy elasticity in linear Cosserat elasticity

It is easy to see that one obtains the linear elasticity displacement solution for $\mu_c = 0$ and $L_c > 0$ in case 1 since the system of equations decouples. For large L_c the microrotations approach a constant value over the entire body if there are no boundary conditions imposed on the microrotations. The system reads

$$\sigma = 2\mu \cdot \operatorname{sym} \overline{\varepsilon} + \lambda \cdot \operatorname{tr}[\overline{\varepsilon}] \cdot \mathbb{1}, \quad m = \gamma \nabla \phi = \mu L_c^2 \nabla \phi, \tag{5.1}$$

$$\operatorname{Div} \sigma = 0, \quad \operatorname{Div} m = 0. \tag{5.2}$$

A second alternative is to take $\mu_c = \mu$ and $L_c = 0$ which, in fact, also represents the linear elasticity solution. Since curvature is absent, the balance of angular momentum equation reduces to the pointwise equation skew $\nabla u = \overline{A}$. Thus the skew-symmetric parts in the balance of force equation cancel and the displacement u is again the Cauchy displacement. In this work, we evaluate these two limit cases by considering $L_c = 1E6\,mm$ and $\mu_c = 0$ for the first case to be sufficiently large in Linear Cosserat (case1) by FEM analysis and it is presented in Figure 12 against the obtained Cauchy solution of the applied identical torsion with the same number of DOFs (DOFs=198618), which nearly presents only 0.14 percent of error. Our numerical results show that our implementation of the Cosserat model perfectly reproduces the linear elastic solution.

5.2 Limit case: Constant infinitesimal mean rotation

Another (more difficult) limit case is $\mu_c > 0$ and $L_c = \infty$ with pointwise positive curvature, case 1 in our curvature classification.[5] From the variational statement of the problem it is clear that the microrotation $\overline{A}$ must be a constant $\widehat{A} \in \mathfrak{so}(3)$ since the energy remains bounded. Minimizing the remaining energy therefore with respect to **constant microrotations** $\widehat{A}$ leads to the problem

$$\int_\Omega \mu \, \| \operatorname{sym} \nabla u \|^2 + \mu_c \, \| \operatorname{skew} \nabla u - \widehat{A} \|^2 + \frac{\lambda}{2} \operatorname{tr}[\nabla u]^2 \, \mathrm{dx} \mapsto \min. \quad (u, \widehat{A}). \tag{5.3}$$

---

[5]In principle the same calculations can be done for conformal curvature. In this case we would be led to consider a ten-dimensional minimization problem for the parameters of the conformal map.
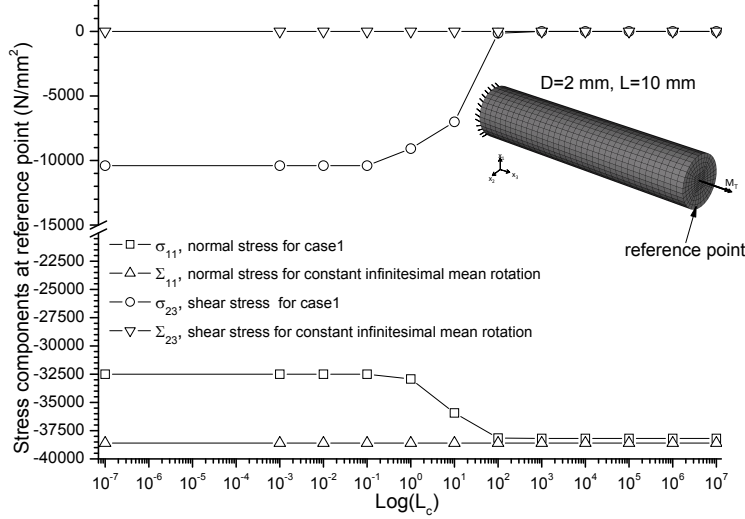
Figure 13: Comparison between the limit solution of constant microrotation, formally $L_c = \infty$ and the Cosserat solution for large L_c.

Thus the equilibrium equation for the constant $\widehat{A} \in \mathfrak{so}(3)$ reads

$$\int_\Omega 2\mu_c \langle \mathrm{skew}\, \nabla u(x) - \widehat{A}, \delta\widehat{A} \rangle \, \mathrm{d}x = 0 \quad \forall \quad \delta\widehat{A} \in \mathfrak{so}(3) \quad \Rightarrow$$

$$\langle \int_\Omega [\mathrm{skew}\, \nabla u(x) - \widehat{A}] \, \mathrm{d}x, \delta\widehat{A} \rangle = 0 \quad \forall \quad \delta\widehat{A} \in \mathfrak{so}(3) \quad \Rightarrow \qquad (5.4)$$

$$\int_\Omega \mathrm{skew}\, \nabla u(x) \, \mathrm{d}x = \int_\Omega \widehat{A} \, \mathrm{d}x = |\Omega|\, \widehat{A} \,.$$

Therefore, the constant microrotation must have the value

$$\widehat{A} = \frac{1}{|\Omega|} \int_\Omega \mathrm{skew}\, \nabla u \, \mathrm{d}x = \mathrm{skew} \left[\frac{1}{|\Omega|} \int_\Omega \nabla u \, \mathrm{d}x \right] = \mathrm{skew} \left[\frac{1}{|\Omega|} \int_{\partial\Omega} u \otimes \vec{n} \, dS \right] \,. \qquad (5.5)$$

Thus the weak problem for the displacement reads then

$$0 = \mathrm{Div}\, \sigma = \mathrm{Div} \left[2\mu\, \mathrm{sym}\, \nabla u + 2\mu_c\, \mathrm{skew}(\nabla u - \widehat{A}) + \lambda \, \mathrm{tr}\, [\nabla u]\, \mathbb{1} \right]$$

$$= \mathrm{Div} \left[2\mu\, \mathrm{sym}\, \nabla u + 2\mu_c\, \mathrm{skew}(\nabla u) + \lambda \, \mathrm{tr}\, [\nabla u]\, \mathbb{1} \right] \,, \qquad (5.6)$$

since $\widehat{A}$ is constant. Hence, once this equation is solved for the torsion-geometry, the stresses σ follow as

$$\sigma = 2\mu\, \mathrm{sym}\, \nabla u + 2\mu_c\, \mathrm{skew}(\nabla u - \widehat{A}) + \lambda \, \mathrm{tr}\, [\nabla u]\mathbb{1} \,. \qquad (5.7)$$

Note that such a formulation is still infinitesimally frame-indifferent because the constant mean rotation filters out the infinitesimal rigid rotation. See Figure 13 for a comparison between this solution and the Cosserat solution for large L_c.

6 Simulation of linear Cosserat elasticity for all three cases

Having amply checked our implementation we are now discussing the simulated response for the linear Cosserat elasticity model. The geometry and the boundary conditions remain the same as previously illustrated in Figure 6. The mesh density and mesh statistics are displayed in Figure 7. We use the exact rotation Dirichlet boundary conditions or so called essential boundary condition as given by (cf. Figure 8):

$$u_1 = 0\,, u_2 = 0\,, u_3 = 0\,, \quad \text{at the bottom} \qquad (6.1)$$

$$u_1 = x \cos\theta + y \sin\theta - x\,, u_2 = -x \sin\theta + y \cos\theta - y\,, u_3 = 0\,, \quad \text{at the top}$$

15

Table 1: Material properties for Cosserat circular bar.

Cases	case1	case2	case3
Young's Modulus $[N/mm^2]$	1E6	1E6	1E6
Poisson's ratio $[-]$	0.3	0.3	0.3
$\mu = \mu_c$ $[N/mm^2]$	$\frac{E}{2(1+\nu)}$	$\frac{E}{2(1+\nu)}$	$\frac{E}{2(1+\nu)}$
λ $[N/mm^2]$	$\frac{\nu E}{(1+\nu)(1-2\nu)}$	$\frac{\nu E}{(1+\nu)(1-2\nu)}$	$\frac{\nu E}{(1+\nu)(1-2\nu)}$
α $[N.mm]$	0	0	$-\frac{\mu L_c^2}{3}$
β $[N.mm]$	0	$\frac{\mu L_c^2}{2}$	$\frac{\mu L_c^2}{2}$
γ $[N.mm]$	μL_c^2	$\frac{\mu L_c^2}{2}$	$\frac{\mu L_c^2}{2}$
L_c $[mm]$	$0 \leq L_c \leq$10E6	$0 \leq L_c \leq$10E6	$0 \leq L_c \leq$10E6

Remember that microrotations $\overline{A} \in \mathfrak{so}(3)$ are not constraint at the boundary. The material parameters for our computations are given in Table 1. The internal length scale parameter L_c will vary from very small values (nearly zero) to very high values ($10E6\,mm$). Since the coupling between microrotations and displacements involves the term $\|\operatorname{curl} u - 2\operatorname{axl}(\overline{A})\|^2$, quadratic elements for u and linear interpolation for $\overline{A}$ have been used in our FEM approach. All computations have been carried out with 198618 DOFs (Figure 7). The results are presented in Figure 14, Figure 15 and Figure 16.

6.1 Pointwise positive case1

We recall here the applied material parameters in curvature energy for this cases: $\frac{\mu L_c^2}{2}\|\nabla\phi\|^2$. This corresponds to $\alpha = 0$, $\beta = 0$, $\gamma = \mu L_c^2$ and the corresponding coupled system of equation is

$$\operatorname{Div}\sigma = 0, \quad \sigma = 2\mu\,\operatorname{sym}(\nabla u - \overline{A}) + 2\mu_c\,\operatorname{skew}(\nabla u - \overline{A}) + \lambda\operatorname{tr}[\overline{\varepsilon}] \cdot \mathbb{1}, \quad (6.2)$$

$$\operatorname{Div} m + 4\mu_c \cdot \operatorname{axl}\operatorname{skew}\overline{\varepsilon} = 0, \quad m = \mu L_c^2 \nabla\phi. \quad (6.3)$$

We appy the exact angle θ on the top from 0 to $\frac{13\pi}{180}$ (rad) for each value of L_c which is varied from zero to $10E6\,mm$. The numerical solution for linear Cosserat elasticity with pointwise positive curvature exhibits more stiffness for higher values of L_c in an asymptotic manner (Figure 14). We observe a bound on the stiffness (the tangent in the plot) for L_c values greater than $100\,mm$ (Figure 14). Case1 reveals significantly more stiffening effects than the other cases (Figure 15 and Figure 16).

6.2 Symmetric case2

The curvature form in Cosserat linear elasticity in this cases is : $\frac{\mu L_c^2}{2}\|\operatorname{sym}\nabla\phi\|^2$ and the moment stress tensor m is also symmetric. The corresponding material parameters are $\alpha = 0$, $\beta = \gamma = \frac{\mu L_c^2}{2}$ and the coupled system of equation is

$$\operatorname{Div}\sigma = 0, \quad \sigma = 2\mu \cdot \operatorname{sym}(\nabla u - \overline{A}) + 2\mu_c \cdot \operatorname{skew}(\nabla u - \overline{A}) + \lambda\operatorname{tr}[\overline{\varepsilon}] \cdot \mathbb{1}, \quad (6.4)$$

$$\operatorname{Div} m + 4\mu_c \cdot \operatorname{axl}\operatorname{skew}\overline{\varepsilon} = 0, \quad m = \mu L_c^2 \cdot \operatorname{sym}\nabla\phi. \quad (6.5)$$

The numerical solution for the linear Cosserat elasticity with symmetric positive curvature exhibits more stiffness for higher values of L_c by an asymptotic manner (Figure 15) as seen before. We observe a bound on the stiffness for L_c values greater than $100\,mm$ (Figure 15).

6.3 Conformal case3

We recall here the relaxed curvature energy in this cases: $\frac{\mu L_c^2}{2}\|\operatorname{dev}\operatorname{sym}\nabla\phi\|^2$. This leads to $\alpha = \frac{-1}{3}\mu L_c^2$, $\beta = \gamma$, $\gamma = \mu L_c^2$ as parameters. Tthe moment stress tensor is symmetric and trace-free and the corresponding coupled system of equations reads

$$\operatorname{Div}\sigma = 0, \quad \sigma = 2\mu \cdot \operatorname{sym}(\nabla u - \overline{A}) + 2\mu_c \cdot \operatorname{skew}(\nabla u - \overline{A}) + \lambda\operatorname{tr}[\overline{\varepsilon}] \cdot \mathbb{1}, \quad (6.6)$$

$$\operatorname{Div} m + 4\mu_c \cdot \operatorname{axl}\operatorname{skew}\overline{\varepsilon} = 0, \quad m = \mu L_c^2 \cdot \operatorname{sym}\nabla\phi - \frac{1}{3}\mu L_c^2\operatorname{tr}[\nabla\phi] \cdot \mathbb{1}. \quad (6.7)$$
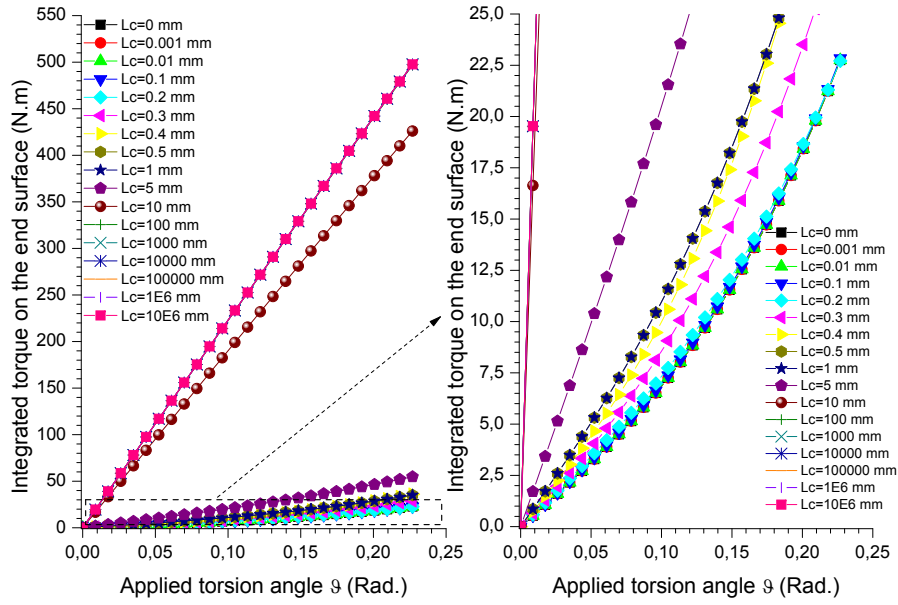
Figure 14: Results for fixed $\mu = \mu_c$ and variation of $L_c[mm]$ for pointwise positive curvature $(D = 2\,mm,\ L = 10\,mm)$.
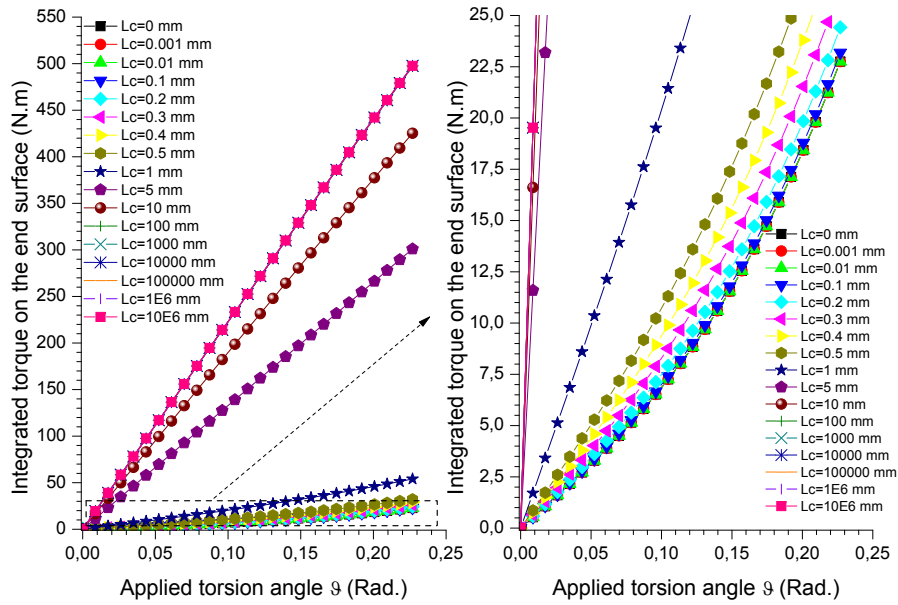
Figure 15: Results for fixed $\mu = \mu_c$ and variation of $L_c[mm]$ for symmetric curvature $(D = 2\,mm,\ L = 10\,mm)$.
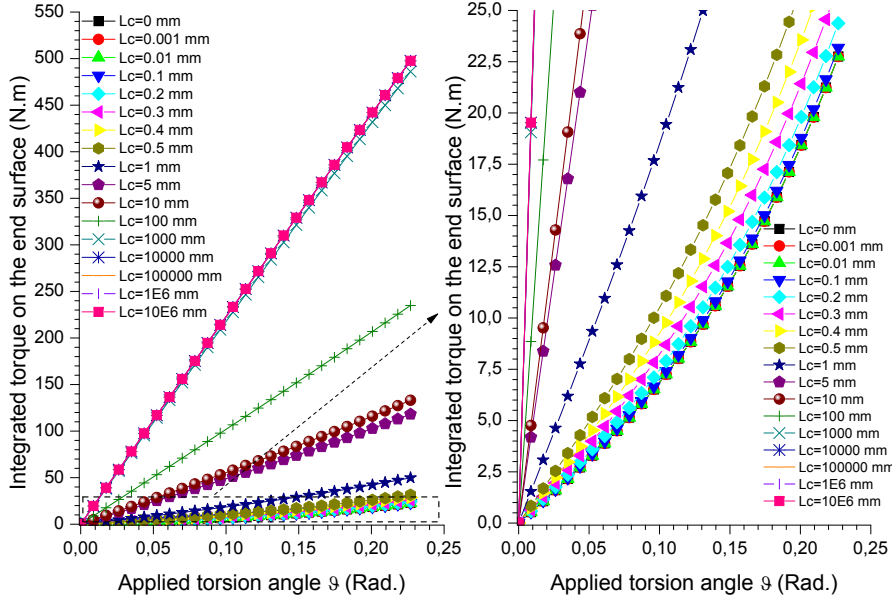
Figure 16: First results for fixed $\mu = \mu_c$ and variation of $L_c[mm]$ for conformal curvature.

The numerical solution for the linear Cosserat elasticity with conformal positive curvature displays again more stiffness for higher values of L_c (Figure 16) and we observe a bound on the stiffness for L_c values now greater than $1000\,mm$ (Figure 16).

6.4 Torque - Log diagram

According to the last results it is possible to plot the torque magnitude at top of cylindrical bar versus "Log(L_c)" in a semi-logarithmic diagram (Figure 17) for a given torsion angle ϑ. In Figure 17, we chose ϑ equal to $13°$ ($\vartheta = \frac{13\pi}{180}\ rad.$) and we plot the Torque-Log(L_c) diagram for all cases (case1, case2 and case3). Evidently, we find the upper and lower bound for the stiffness M_T. In the diagram we distinguish three specific zones: **Zone I** tends toward linear Cauchy elasticity with no size effects present, **Zone II** is an intermediate zone in which the size effects appear and we can clearly distinguish the Cosserat effects for our numerical models, **Zone III** describes a situation where the microrotation is nearly constant with the limit behavior discussed explicitly in section 5.2. The most interesting zone is the intermediate Zone II. We see that the pattern given for case1 and case2 has been disturbed beyond Zone I in case3 and only later it gets the expected pattern (Figure 18). This distinguishing phenomenon for case3 means less stiffening effects and a more pronounced size effect (the spread between linear elasticity and constant mean rotation, i.e. where size-dependent response occurs covers orders of magnitude larger L_c-values).

The case1 and case2 show practically the same behavior in this Torque-Log(L_c) diagram, whereas case3 behaves in a completely different manner. This is due to the fact that we have the third constitutive parameter ($\alpha = -\frac{\mu L_c^2}{3} \neq 0$) for the couple stress-curvature tensor constitutive law. From our numerical experiments we observe that case 2 and case 3 are numerically more stable than case1 in the sense that better convergence rates have always been observed with a consistent runtime reduction. Surprisingly, for case 1, at the beginning of Zone II, we have observed some numerical instabilities (in the range $0.5 \leq L_c \leq 0.75\,mm$). Thus our numerical results suggest that the weaker the curvature energy is chosen (case 2 or case 3) the better the convergence as compared to the pointwise positive case. The torque-log diagram indicates a completely different size-effect response for the conformal case. It can be seen that then a much larger L_c-value can be taken to produce the same amount of torque at equal applied rotation angle. Thus, in an inverse calculation for the determination of the characteristic size (related to L_c), we may obtain these larger L_c-values. A typical problem in the parameter-fitting of based on case1 is that there the fitted L_c-values would be orders of magnitude smaller than anything which could physically serve as setting a characteristic size.
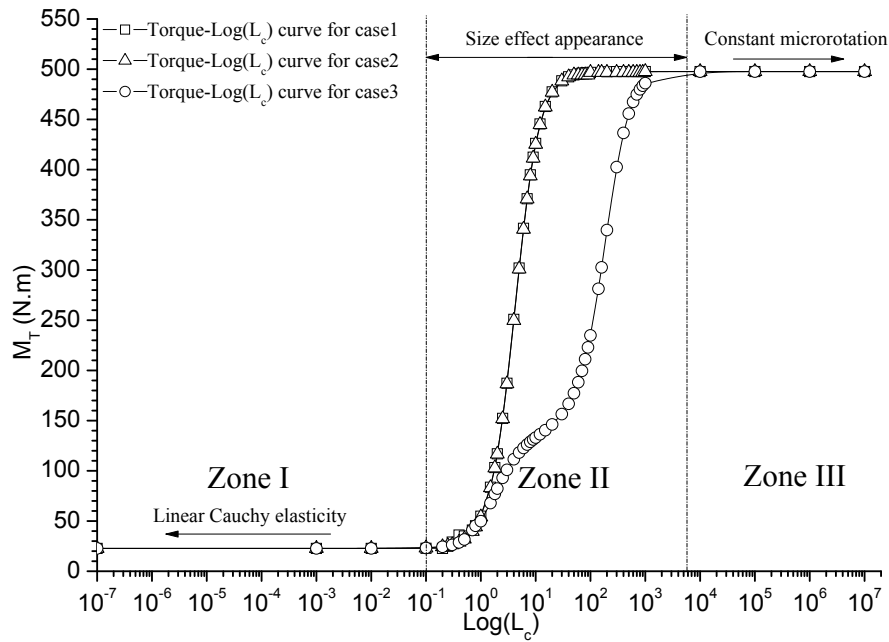
Figure 17: Torque versus L_c in a semi-logarithmic diagram $(M_T - Log(L_c))$ for the cylindrical bar (L=10 mm and D=2 mm) and $\vartheta = 13° = \frac{13\pi}{180} \ rad$.
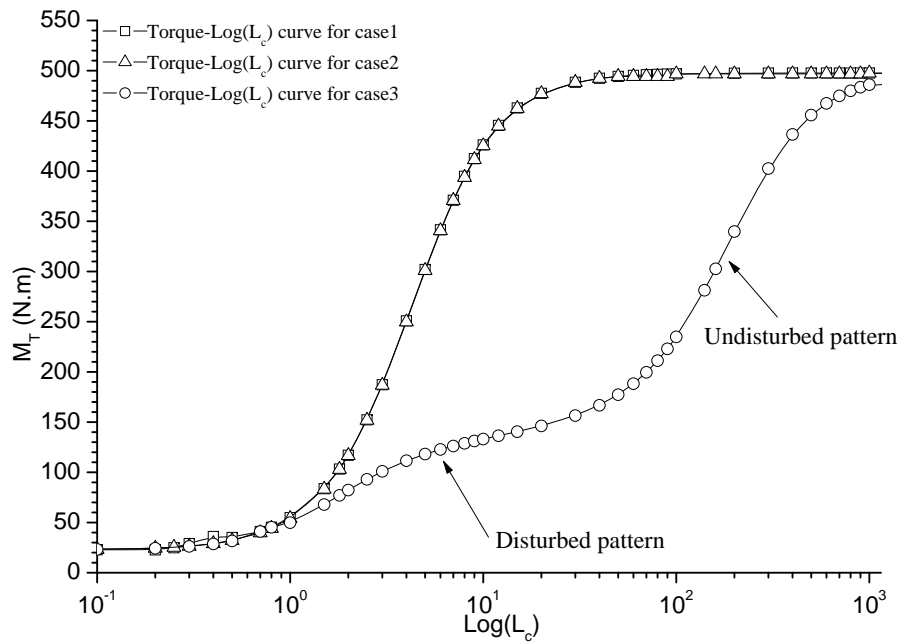
Figure 18: **Zone II** of $M_T - Log(L_c)$ diagram for the cylindrical bar (L=10 mm and D=2 mm) and $\vartheta = 13° = \frac{13\pi}{180} \ rad$.

7 Discussion

The reduction in Cosserat parameters from six to four in the 3D-case which is embodied in the conformal case3 is necessitated by the physical principle of bounded stiffness for very small samples and the use of the analytical solution formulas for these cases, see [9]. It remains to be investigated whether conformal invariance is, in fact, a more primitive physical concept, perhaps to be motivated by novel invariance principles, with consequences for the Cosserat model. Here, we have shown that the novel conformal model allows for a consistent numerical treatment and is therefore ready to use in practical applications. By comparing it with the more standard Cosserat approach (case1) we have demonstrated that the novel conformal model (case3) still shows a size-effect, which is, however, completely different than the traditional one with pointwise positive curvature (case1) or symmetric curvature (case2) of our classification. It allows for dramatically increased values of the internal length scale L_c still giving us a size effect in torsion and not constraining the microrotation to be constant over the sample for larger L_c-values.

We think that the conformal curvature expression offers a fresh departure for the experimental determination of the remaining two Cosserat constants: one internal length scale L_c and one coupling constant μ_c. We hope that other groups will take up this route as well and provide finally physically consistent parameter values for the linear Cosserat model for specific materials.

In a future contribution we will investigate the infinitesimal indeterminate couple stress problem (formally $\mu_c = \infty$) with conformal curvature.

References

[1] M. Baluch, J.E. Goldberg, and S.L. Koh. Finite element approach to plane microelasticity. *J. of Structural Division-American Society of Civil Engineering*, 98:1957–1964, 1972.

[2] S. Diebels and H. Steeb. The size effect in foams and its theoretical and numerical investigation. *Proc. R. Soc. London A*, 458:2869–2883, 2002.

[3] S. Diebels and H. Steeb. Stress and couple stress in foams. *Comp. Mat. Science*, 28:714–722, 2003.

[4] A. Dietsche, P. Steinmann, and K. Willam. Micropolar elastoplasticity and its role in localization. *Int. J. Plasticity*, 9:813–831, 1993.

[5] W. Ehlers, S. Diebels, and W. Volk. Deformation and compatibilty for elasto-plastic micropolar materials with applications to geomechanical problems. In A. Bertram and F. Sidoroff, editors, *Mechanics of Materials with Intrinsic Length Scale: Physics, Experiments, Modelling and Applications.*, Journal Physique IV France 8, pages 127–134. EDP Sciences, France, 1998.

[6] P. Grammenoudis and C. Tsakmakis. Finite element implementation of large deformation micropolar plasticity exhibiting isotropic and kinematic hardening effects. *Int. J. Num. Meth. Engng.*, 62(12):1691–1720, 2005.

[7] P. Grammenoudis and C. Tsakmakis. Predictions of microtorsional experiments by micropolar plasticity. *Proc. Roy. Soc. London A*, 461:189–205, 2005.

[8] F.Y. Huang, B.H. Yan, J.L. Yan, and D.U. Yang. Bending analysis of micropolar elastic beam using a 3-d finite element method. *Int. J. Engng. Sci.*, 38:275–286, 2000.

[9] J. Jeong and P. Neff. Existence, uniqueness and stability in linear Cosserat elasticity for weakest curvature conditions. *Preprint 2550, http://www3.mathematik.tu-darmstadt.de/fb/mathe/bibliothek/preprints.html, to appear in Math. Mech. Solids*, 2008.

[10] C.S. Jog. Higher-order shell elements based on the Cosserat model, and their use in the topology design of strutures. *Comp. Meth. Appl. Mech. Engng.*, 193:2191–2220, 2004.

[11] A.R. Khoei, A.R. Tabarraie, and A.A. Gharehbaghi. H-adaptive mesh refinement for shear band localization in elasto-plasticity Cosserat continuum. *Commun. Nonlinear Sci. Numer. Simul.*, 10:253–286, 2005.

[12] L. Li and S. Xie. Finite element method for linear micropolar elasticity and numerical study of some scale effects phenomena in MEMS. *Int. J. Mech. Sci.*, 46:1571–1587, 2004.

[13] X. Li and H. Tang. A consistent return mapping algorithm for pressure-dependent elastoplastic Cosserat continua and modelling of strain localizaton. *Comput. Structures*, 83(1):1–10, 2005.

[14] P. M. Mariano and F.L. Stazi. Computational aspects of the mechanics of complex materials. *Arch. Comput. Meth. Engng.*, 12:392–478, 2005.

[15] I. Münch. *Ein geometrisch und materiell nichtlineares Cosserat-Modell - Theorie, Numerik und Anwendungmöglichkeiten.* Dissertation in der Fakultät für Bauingenieur-, Geo- und Umweltwissenschaften, ISBN 978-3-935322-12-6, electronic version available at http://digbib.ubka.uni-karlsruhe.de/volltexte/1000007371, Karlsruhe, 2007.

[16] B. Nadler and M.B. Rubin. A new 3-d finite element method for nonlinear elasticity using the theory of a Cosserat point. *Int. J. Solids Struct.*, 40:4585–4614, 2003.

[17] S. Nakamura, R. Benedict, and R. Lakes. Finite element method for orthotropic micropolar elasticity. *Int. J. Engng. Sci.*, 22:319–330, 1984.

[18] P. Neff. The Cosserat couple modulus for continuous solids is zero viz the linearized Cauchy-stress tensor is symmetric. *Preprint 2409, http://www3.mathematik.tu-darmstadt.de/fb/mathe/bibliothek/preprints.html, Zeitschrift f. Angewandte Mathematik Mechanik (ZAMM)*, 86(DOI 10.1002/zamm.200510281):892–912, 2006.

[19] P. Neff. Existence of minimizers for a finite-strain micromorphic elastic solid. *Preprint 2318, http://www3.mathematik.tu-darmstadt.de/fb/mathe/bibliothek/preprints.html, Proc. Roy. Soc. Edinb. A*, 136:997–1012, 2006.

[20] P. Neff, K. Chełmiński, W. Müller, and C. Wieners. A numerical solution method for an infinitesimal elastic-plastic Cosserat model. *Preprint 2470, http://www3.mathematik.tu-darmstadt.de/fb/mathe/bibliothek/preprints.html, Math. Mod. Meth. Appl. Sci. (M3AS)*, 17(8):1211–1239, 2007.

[21] P. Neff and S. Forest. A geometrically exact micromorphic model for elastic metallic foams accounting for affine microstructure. Modelling, existence of minimizers, identification of moduli and computational results. *J. Elasticity*, 87:239–276, 2007.

[22] P. Neff and J. Jeong. The linear isotropic Cosserat model with conformally invariant curvature energy. *Preprint 258?, http://www3.mathematik.tu-darmstadt.de/fb/mathe/bibliothek/preprints.html, in preparation*, 2008.

[23] E. Providas and M.A. Kattis. Finite element method in plane Cosserat elasticity. *Comp. Struct.*, 80:2059–2069, 2002.

[24] M. Ristinmaa and M. Vecchi. Use of couple-stress theory in elasto-plasticity. *Comp. Meth. Appl. Mech. Engrg.*, 136:205–224, 1996.

[25] R.S. Rivlin. The formulation of theories in generalized continuum mechanics and their physical significance. *Symposia in Mathematica*, 1:357–373, 1969.

[26] E. Sharbati and R. Naghdabadi. Computational aspects of the Cosserat finite element analysis of localization phenomena. *Comput. Mat. Science*, 38:303–315, 2006.

[27] R. Stojanovic. On the mechanics of materials with microstructure. *Acta Mechanica*, 15:261–273, 1972.

[28] P. Trovalusci and R. Masiani. Non-linear micropolar and classical continua for anisotropic discontinuous materials. *Int. J. Solids Struct.*, 40(5):1281–1297, 2003.

[29] F. Yang, A.C.M. Chong, D.C.C. Lam, and P. Tong. Couple stress based strain gradient theory for elasticity. *Int. J. Solids Struct.*, 39:2731–2743, 2002.

[30] B. Zastrau. *Zur Berechnung orientierter Kontinua - Entwicklung einer Direktorentheorie und Anwendung der Finiten Elemente.* Number 4/60 in Fortschrittberichte der VDI Zeitschriften. Verein Deutscher Ingenieure, VDI-Verlag GmbH, Düsseldorf, 1981.

[31] B. Zastrau and H. Rothert. Herleitung einer Direktortheorie für Kontinua mit lokalen Krümmungseigenschaften. *Z. Angew. Math. Mech.*, 61:567–581, 1981.

Notation

Let $\Omega \subset \mathbb{R}^3$ be a bounded domain with Lipschitz boundary $\partial\Omega$ and let Γ be a smooth subset of $\partial\Omega$ with non-vanishing 2-dimensional Hausdorff measure. For $a, b \in \mathbb{R}^3$ we let $\langle a, b\rangle_{\mathbb{R}^3}$ denote the scalar product on $\mathbb{R}^3$ with associated vector norm $\|a\|^2_{\mathbb{R}^3} = \langle a, a\rangle_{\mathbb{R}^3}$. We denote by $\mathbb{M}^{3\times 3}$ the set of real 3×3 second order tensors, written with capital letters and Sym denotes symmetric second orders tensors. The standard Euclidean scalar product on $\mathbb{M}^{3\times 3}$ is given by $\langle X, Y\rangle_{\mathbb{M}^{3\times 3}} = \text{tr}\left[XY^T\right]$, and thus the Frobenius tensor norm is $\|X\|^2 = \langle X, X\rangle_{\mathbb{M}^{3\times 3}}$. In the following we omit the index $\mathbb{R}^3, \mathbb{M}^{3\times 3}$. The identity tensor on $\mathbb{M}^{3\times 3}$ will be denoted by $\mathbb{1}$, so that $\text{tr}\left[X\right] = \langle X, \mathbb{1}\rangle$. We set $\text{sym}(X) = \frac{1}{2}(X^T + X)$ and $\text{skew}(X) = \frac{1}{2}(X - X^T)$ such that $X = \text{sym}(X) + \text{skew}(X)$. For $X \in \mathbb{M}^{3\times 3}$ we set for the deviatoric part $\text{dev}\,X = X - \frac{1}{3}\text{tr}\left[X\right]\mathbb{1} \in \mathfrak{sl}(3)$ where $\mathfrak{sl}(3)$ is the Lie-algebra of traceless matrices. The set $\text{Sym}(n)$ denotes all symmetric $n \times n$-matrices. The Lie-algebra of $SO(3) := \{X \in GL(3) \mid X^T X = \mathbb{1}, \det[X] = 1\}$ is given by the set $\mathfrak{so}(3) := \{X \in \mathbb{M}^{3\times 3} \mid X^T = -X\}$ of all skew symmetric tensors. The canonical identification of $\mathfrak{so}(3)$ and $\mathbb{R}^3$ is denoted by $\text{axl}\,\overline{A} \in \mathbb{R}^3$ for $\overline{A} \in \mathfrak{so}(3)$. Note that $(\text{axl}\,\overline{A}) \times \xi = \overline{A}.\xi$ for all $\xi \in \mathbb{R}^3$, such that

$$\text{axl}\begin{pmatrix} 0 & \alpha & \beta \\ -\alpha & 0 & \gamma \\ -\beta & -\gamma & 0 \end{pmatrix} := \begin{pmatrix} -\gamma \\ \beta \\ -\alpha \end{pmatrix}, \quad \overline{A}_{ij} = \sum_{k=1}^3 -\varepsilon_{ijk} \cdot \text{axl}\,\overline{A}_k,$$

$$\|\overline{A}\|^2_{\mathbb{M}^{3\times 3}} = 2\|\text{axl}\,\overline{A}\|^2_{\mathbb{R}^3}, \qquad \langle\overline{A}, \overline{B}\rangle_{\mathbb{M}^{3\times 3}} = 2\langle\text{axl}\,\overline{A}, \text{axl}\,\overline{B}\rangle_{\mathbb{R}^3}, \tag{7.1}$$

where ε_{ijk} is the totally antisymmetric permutation tensor. Here, $\overline{A}.\xi$ denotes the application of the matrix $\overline{A}$ to the vector ξ and $a \times b$ is the usual cross-product. Moreover, the inverse of axl is denoted by anti and defined by

$$\begin{pmatrix} 0 & \alpha & \beta \\ -\alpha & 0 & \gamma \\ -\beta & -\gamma & 0 \end{pmatrix} := \text{anti}\begin{pmatrix} -\gamma \\ \beta \\ -\alpha \end{pmatrix}, \quad \text{axl}(\text{skew}(a \otimes b)) = -\frac{1}{2}\,a \times b, \tag{7.2}$$

and

$$2\,\text{skew}(b \otimes a) = \text{anti}(a \times b) = \text{anti}(\text{anti}(a).b). \tag{7.3}$$

Moreover,

$$\text{curl}\,u = 2\,\text{axl}(\text{skew}\,\nabla u). \tag{7.4}$$

By abuse of notation we denote the differential $D\varphi$ of the deformation $\varphi : \mathbb{R}^3 \mapsto \mathbb{R}^3$ by $\nabla\varphi$. This implies a transposition in certain comparisons with other literature since here $(\nabla\varphi)_{ij} = \partial_j\varphi^i$ is understood.